

# A structural instability drives the VO<sub>2</sub> metal-insulator transition

Javier del Valle<sup>1,2\*</sup>, Carl Willem Rischau<sup>3</sup>, Artem Korshunov<sup>4</sup>, David Ambrosi<sup>1</sup>, Aitana Tarazaga Martín-Luengo<sup>1,2</sup>, Ibraheem Yousef<sup>6</sup>, Sara A. Lopez-Paz<sup>5</sup>, Shany Neyshtadt-Ronel<sup>7</sup>, Stefano Gariglio<sup>3</sup>, Alexei Bosak<sup>4</sup>, Sonia Francoual<sup>8</sup> and Yoav Kalcheim<sup>7</sup>

<sup>1</sup>Department of Physics, University of Oviedo, C/ Federico García Lorca 18, 33007 Oviedo, Spain

<sup>2</sup>Center of Research on Nanomaterials and Nanotechnology, CINN (CSIC-Universidad de Oviedo), El Entrego 33940, Spain

<sup>3</sup>Department of Quantum Matter Physics, University of Geneva, 24 Quai Ernest-Ansermet, 1211 Geneva, Switzerland

<sup>4</sup>European Synchrotron Radiation Facility, BP 220, 38043 Grenoble Cedex, France

<sup>5</sup>Department of Chemistry, University of Copenhagen, Universitetsparken 5, 2100 Copenhagen, Denmark

<sup>6</sup>MIRAS Beamline BL01, ALBA-CELLS Synchrotron, Cerdanyola del Vallès, 08209, Barcelona, Spain

<sup>7</sup>Department of Material Science and Engineering, Technion - Israel Institute of Technology, Haifa 32000, Israel

<sup>8</sup>Deutsches Elektronen-Synchrotron (DESY), Notkestraße 85, 22607 Hamburg, Germany

\*Corresponding author: javier.delvalle@uniovi.es

## Abstract

VO<sub>2</sub> features concomitant structural and metal-insulator transitions. This poses a challenge for understanding the underlying mechanism: is the transition triggered by a structural or by an electronic instability? Here, we address this question by studying pre-transitional fluctuations in the metallic state. By measuring resonant diffuse X-ray scattering we find no evidence that spatial fluctuations of *d*-electrons are any different from those of vanadium ion cores. That is, charge and lattice remain coupled as they fluctuate jointly towards the insulating phase, strongly supporting the case that the VO<sub>2</sub> metal-insulator transition is triggered by a structural instability. Our work offers a novel approach to solve similar problems in other strongly correlated systems.

## Introduction

Many strongly correlated materials feature phase transitions in which both the electronic and structural order parameters change simultaneously. Concomitant electronic and structural transitions are observed in systems as diverse as Kagome metals [1], colossal magnetoresistance manganites [2], charge density wave dichalcogenides [3,4] or metal-insulator transition (MIT) oxides [5–7]. In all these cases, understanding the driving force triggering the transition is complicated due to coincident changes in spin, charge, and lattice ordering. Two scenarios are generally proposed: the transition is induced either by a lattice instability or by an electronic

instability [8–10]. Figure 1 shows a schematic representation of both scenarios in terms of free energy, an analysis inspired by recent work by Georgescu *et al.* [8].

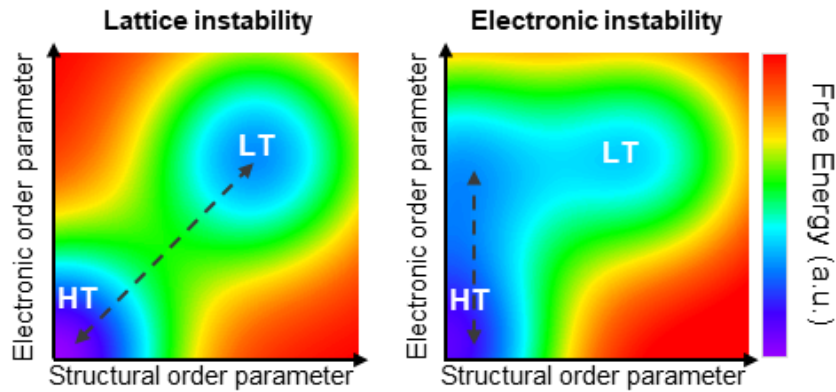


Figure 1. Schematic representation of the two scenarios proposed to describe concomitant electronic and structural transitions. The free energy is plotted as a function of two order parameters: the structural and the electronic. The two local minima correspond to the high (HT) and low temperature (LT) phases. In this specific example,  $T > T_C$ , so the undistorted HT phase is the global minimum and the LT phase is metastable. Dashed arrows show the fluctuations from the HT phase expected for the two scenarios.

In the lattice instability picture, both the ion cores and valence electrons reorganize jointly to reduce the overall energy of the system [8]. One example of such instability would be the Peierls transition. In the electronic instability picture, electronic interactions alone reorder the configuration of valence electrons, without the need for a lattice deformation [11,12]. A classic example is the metal-insulator transition of the Mott-Hubbard model [13]. In this later case, the lattice could still deform, but only as a consequence of the valence electron redistribution. Since the lattice follows the electronic charge in timescales as fast as 100 fs [14], it is very challenging to experimentally differentiate between the two scenarios. This egg-or-chicken problem has resulted in a longstanding debate in the condensed matter community.

$\text{VO}_2$  is a paradigmatic example of this dilemma, undergoing a phase transition from a rutile paramagnetic metal into a monoclinic diamagnetic insulator at 340 K [7,15]. These are usually termed the R and M1 phases, respectively. In the M1 phase, all vanadium atoms dimerize, electrons form singlet pairs, and the resulting large interdimer hopping renders the system insulating. Goodenough made the first theoretical description of the transition, proposing the bonding-antibonding splitting induced by dimerization as the key element opening the insulating gap [16]. This is schematically described in Figure S1a,b [17]. Later calculations showed that while this lattice-driven picture is conceptually correct, it is necessary to include strong electron-electron correlations for the insulating gap to open [9,10,18], making the MIT a correlations-assisted Peierls transition. Such a picture would still be described by the left panel in Figure 1.

The discovery of a second monoclinic insulating phase (M2 phase, see phase diagram in Fig. S1c), where only half of the vanadium atoms dimerize [19], challenged the naïve lattice-driven picture and suggested that electron-electron interactions might dominate [20–22]. DFT/DMFT calculations placed the R phase near a Mott instability [20], and further experiments showed this

phase to be a strongly correlated metal on the brink of localization. This was evidenced by a resistivity above the Ioffe-Regel limit [23], Planckian dissipation [24], the presence of a pseudogap [25,26] and exotic thermal transport signatures [27]. More recent experiments have even proposed that the MIT and structural transitions of VO<sub>2</sub> and the related compound V<sub>2</sub>O<sub>3</sub> can take place independently [12,28–31], although these results have subsequently been challenged, both in the equilibrium [32–34] and ultrafast regimes [35]. Despite decades of research, a consensus on what triggers the VO<sub>2</sub> MIT is still lacking, exemplifying the broader challenge of understanding coupled electronic and structural phenomena in correlated materials.

Here, we tackle the problem by following a new approach: studying fluctuations in the metallic R phase above the MIT temperature. By focusing on pre-transitional dynamics, we aim to indirectly probe the free energy landscape shown in Figure 1, since the two outlined scenarios should feature very different fluctuations. The shape of the free energy allows for large charge fluctuations with little lattice distortion in the case of an electronic instability, while charge and lattice are bound to move jointly in the case of a lattice instability (dashed arrows in Figure 1).

We begin by demonstrating that both the electronic and structural properties of the R phase exhibit strong fluctuations towards the low temperature insulating phase. We then show X-ray diffuse scattering measurements across the vanadium K-edge, which allow us to directly compare the spatial pattern of fluctuations associated with *d* valence electrons and vanadium ion cores. Since the scattering time at the vanadium K-edge (~1 fs [36]) is faster than typical electronic and lattice timescales, any decoupling between charge and structure would be captured in the diffraction pattern. Our results reveal no differences between resonant and non-resonant scattering, indicating that charge and lattice remain tightly coupled as they fluctuate. This result strongly supports the conclusion that the MIT in VO<sub>2</sub> is triggered by a structural instability. Moreover, our findings establish a methodology to experimentally address similar problems in other strongly correlated materials beyond MITs.

### **Pre-transitional electronic fluctuations**

We fabricated VO<sub>2</sub> single crystals using the self-flux method, annealing V<sub>2</sub>O<sub>5</sub> powder for 24 hours at 1000° C under an Argon gas flow [37]. High quality single crystals with lengths up to several mm can be obtained this way.

Figure 2a shows the resistivity vs temperature (*T*) of one of these crystals, which undergoes a five orders of magnitude resistivity change at the MIT. The inset in Figure 2a presents infrared reflectance measurements in the R phase, performed at the MIRAS beamline at the ALBA synchrotron. The spectral feature near 0.2 eV, located well above the phonon spectrum, corresponds to the pseudogap previously reported by Qazilbash et al. [25] and Huffman et al. [26]. The presence of a pseudogap suggests that in the metallic state, conduction electrons are not completely itinerant, but are partially localized. Similar pseudogaps have been reported in the metallic state of related MIT compound V<sub>2</sub>O<sub>3</sub> [38].

Figure 2b shows magnetic susceptibility ( $\chi$ ) as a function of temperature (300 K - 1000 K). The diamagnetic to paramagnetic transition is readily visible close to 340 K. Surprisingly, the paramagnetic  $\chi$  has a strong temperature dependence. This is unexpected for metals, usually

dominated by temperature-independent Pauli paramagnetism [39]. The inset in Figure 2b shows  $\chi^{-1}$  vs  $T$ . Although not quite linear in temperature, a behavior reminiscent of Curie paramagnetism can be appreciated, again indicating that conduction electrons are partially localized. The slope of the  $\chi^{-1}(T)$  curve is not constant but becomes flatter as the MIT is approached. A crude extrapolation results in a negative temperature intercept for  $\chi^{-1}=0$ , consistent with antiferromagnetic correlations [39] that would favor the formation of spin singlets. Together, the resistivity and the magnetic susceptibility results suggest the presence of localized conduction electrons and the emergence of pre-transitional spin singlets in the R phase of VO<sub>2</sub>.

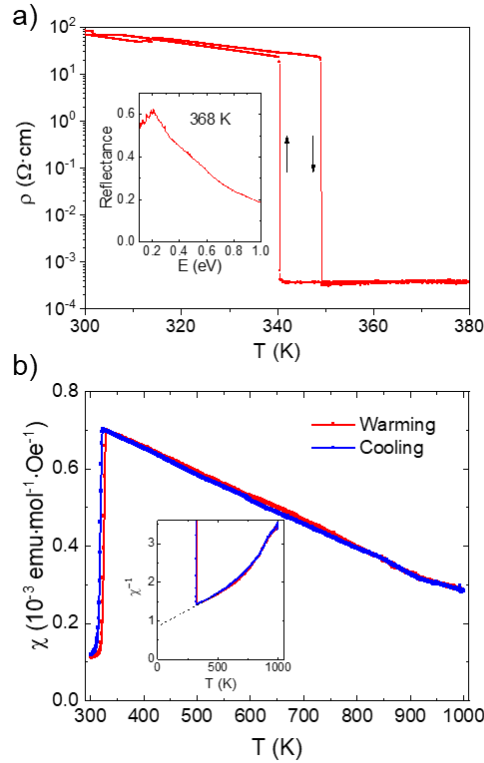


Figure 2. a) Resistivity vs  $T$ . Inset: Infrared reflectance vs photon energy measured in the R phase at  $T=368$  K. b)  $\chi$  vs  $T$ . Inset:  $\chi^{-1}$  vs  $T$ . The dashed line is an extrapolation obtained by a linear fitting of the 350 K – 550 K range.

### Pre-transitional structural fluctuations

Metallic VO<sub>2</sub> features a rutile structure consisting of chains of edge-sharing VO<sub>6</sub> octahedra interconnected via the apical oxygen, as shown in Figure S2 [17]. The strongest structural correlations are thus contained within the  $(\pm 1 \pm 1 0)_R$  planes [40]. Figure 3a shows the structure of the R, M2, and M1 phases in the  $(1-1 0)_R$  plane. As pointed out by Pouget *et al.* [7], the M2 structure can be derived from the R structure by considering 1-dimensional, chain-like shifts of vanadium positions along the  $[11 \pm 1]_R$  and  $[-1-1 \pm 1]_R$  directions. These are represented with black arrows. The interchain interaction results in the M2 structure: dimerization and buckling along  $[001]_R$ , as schematically depicted in the central panel of Figure 3a. The M1 structure can be further

derived from the M2 phase by also including chain-like shifts in the perpendicular plane, along the  $[1-1\pm 1]_R$  and  $[-11\pm 1]_R$  directions [7,40].

Pre-transitional, one-dimensional  $[\pm 1\pm 1\pm 1]_R$  displacements can be strikingly visualized with diffuse X-ray scattering. Chain-like disorder is expected to manifest as 2-dimensional planes of diffuse scattering in reciprocal space. Figure 3b shows total X-ray scattering measurements performed in ID28 at the ESRF using a photon energy of 15.8 keV. Reciprocal space slices parallel to the (HK0) plane, as well as the (HHL) plane are displayed. In addition to the Bragg peaks from the average rutile structure, intense streaks of diffuse scattering can be seen. These correspond to intercepts of diffuse scattering planes oriented perpendicularly to the  $[\pm 1\pm 1\pm 1]_R$  directions. As previously shown [37,41,42], these planes do not arise from static disorder but from dynamical fluctuations that become softer as the MIT is approached. They pass through the  $R$  and  $M$  high symmetry points (see Figure S3 [17] for a schematic representation of the R phase Brillouin zone).

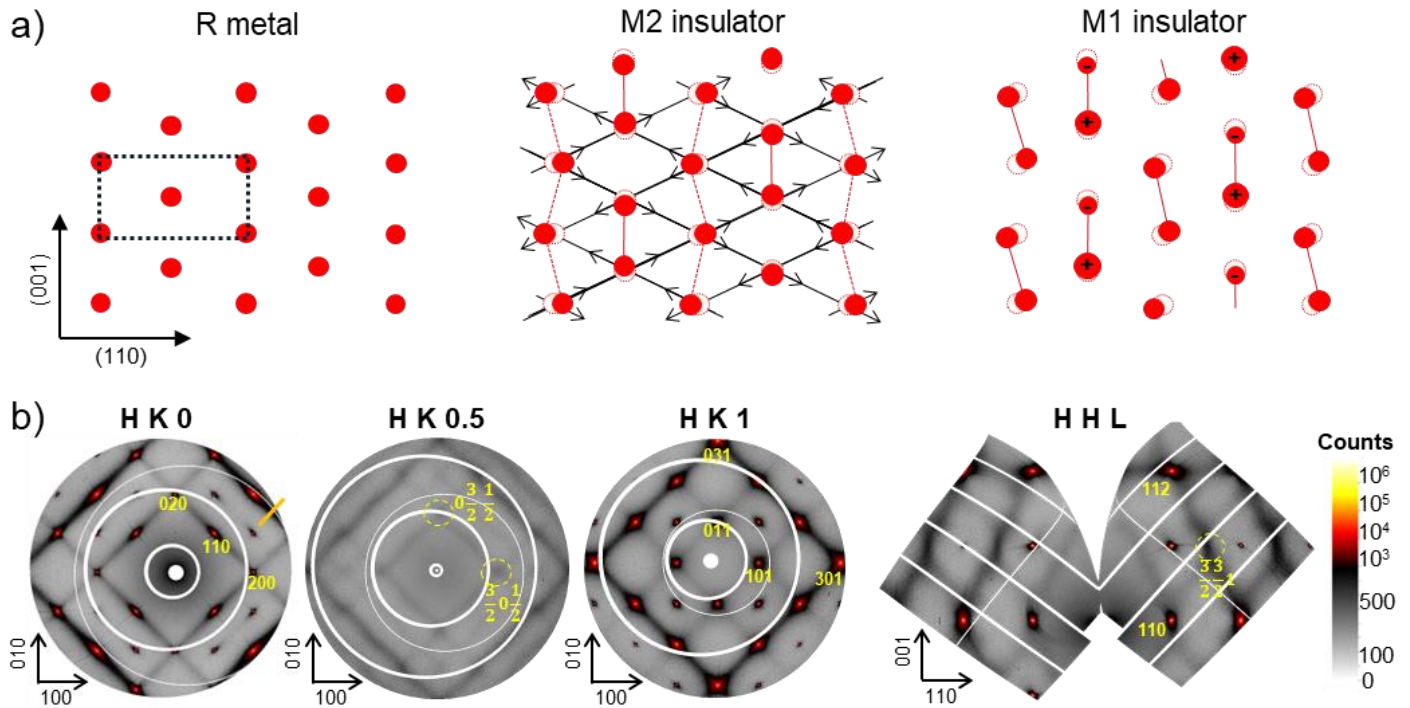


Figure 3. a) Schematic representation of the structure of the R, M2, and M1 phases, viewed in the (1 -1 0) plane. Solid red circles represent Vanadium atoms. Dashed empty circles show the original position of the vanadium atoms in the R-phase. Black arrows show the alternating chain-like displacements along the  $[11\pm 1]_R$  and  $[-1-1\pm 1]_R$  directions. Solid circles with - and + signs indicate displacements in and out of the page. The dotted rectangle shows the basic unit cell in the R phase b) X-ray total scattering in different slices of the reciprocal space, measured in the R phase at 350 K: HK0, HK0.5, HK1, and HHL. Several Bragg peaks and high symmetry  $M$  and  $R$  points are outlined in yellow.

## Resonant diffuse X-ray scattering

Results shown in Figures 2 and 3 establish that, within the metallic R phase, there are strong electronic and structural fluctuations towards the M1/M2 phases. However, the different probes used do not allow a direct comparison of charge and lattice fluctuations, which is critical for distinguishing between the two scenarios depicted in Figure 1. Resonant Elastic X-ray scattering (REXS) provides an ideal tool for this task. Off-resonance scattering is mainly determined by the positions of ion cores, and therefore provides information about the lattice. Resonant scattering, on the other hand, features extra intensity coming from the position of valence orbitals, and it is commonly used to detect electronic ordering [43–45] and dynamic correlations [46]. Therefore, by measuring diffuse X-ray scattering in and out of resonance, we can directly probe whether charge fluctuations are stronger or follow a different spatial pattern than lattice fluctuations.

We performed REXS measurements at the P09 beamline at PETRA III at DESY, with an energy resolution of around 0.7 eV. Since the Vanadium L-edge does not provide enough photon momentum to probe the areas of reciprocal space where the diffuse scattering planes are located, we used the Vanadium K-edge (5.47 keV) for our experiment. The  $1s \rightarrow 3d$  transition is allowed by quadrupolar effects. The vanadium K pre-edge has been shown to be very sensitive to the oxidation state and the MIT [47], and REXS has successfully been applied to detect magnetic and orbital ordering in  $V_2O_3$  [44].

Figure 4a shows (H,H,0) line scans for three photon energies: off-resonance, the K pre-edge, and the K main-edge. The scan trajectory across reciprocal space, marked by an orange bar in the leftmost panel of Figure 3b, intersects a diffuse scattering plane at the  $M$  point. The broad feature corresponds to the cross-section of the plane, while the sharp peak at  $H=1.67$  originates from beryllium powder lines coming from the vacuum dome. Notably, the shape and width of the diffuse scattering signal remains unchanged across the K edge. Measurements were performed with light polarized along the rutile  $c$ -axis to maximize sensitivity to the  $d_{||}$  orbital [48] (see Figure S1 [17]). Data in Figure 4 were acquired in the  $\sigma$ - $\sigma'$  configuration, that is, detecting the unrotated polarization component of the scattered light. Additional results from the  $\sigma$ - $\pi'$  channel as well as other sample azimuths are shown in the supplementary information and Figure S4 [17].

Figure 4b shows the intensity vs photon energy at several reciprocal space points: the Bragg reflection (3 0 -1) and two  $M$  and  $R$  high symmetry points contained within the diffuse scattering planes. At the top of the panel, the fluorescence signal, proportional to the sample absorption, is plotted. As the K edge is crossed, the sample starts absorbing X-rays, reducing the overall number of scattered photons leaving the sample. The effect of absorption can be seen in the energy dependence of the (3 0 -1) Bragg reflection, which decreases by a factor of five across the K-edge. The  $R$  and  $M$  points mimic the same energy dependence, dominated by the sample absorption. The same is observed for the other three high symmetry points not contained in the diffuse scattering planes, as well as for a background point (0 3.5 -0.25). These are shown in Figure S5 [17]. Crucially, no enhancement close to the absorption edge, commonly seen when there is charge ordering, is detected at the (111) scattering planes or any high symmetry point of the R-phase structure.

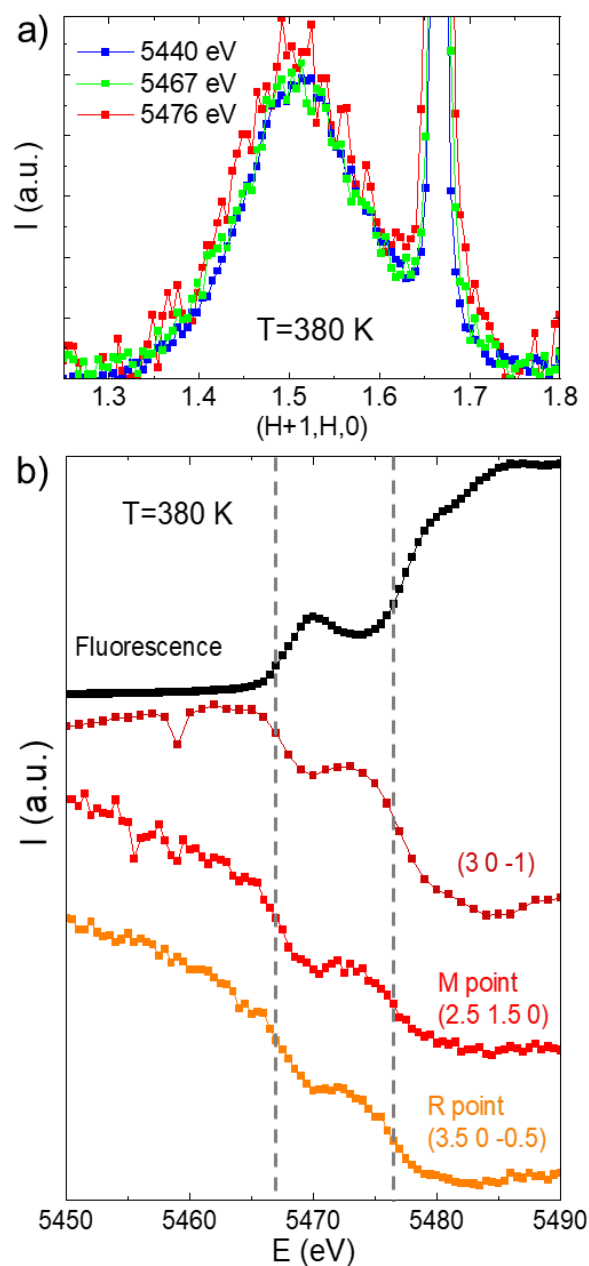


Figure 4. a) X-ray diffuse scattering along a line scan, following the path outlined with an orange line on the leftmost panel of Figure 3b. Three energies are shown: 30 eV below the absorption edge, at the pre-edge, and at the edge. The sharp feature originates from a Beryllium powder line. The scan intensity has been normalized to better compare the scan shape. b) Top curve: Fluorescence signal vs photon energy. Other curves: X-ray intensity vs photon energy in the  $\sigma$ - $\sigma'$  channel for different points in reciprocal space: the Bragg reflection (3 0 -1) and two  $M$  and  $R$  high symmetry points contained within the diffuse scattering planes.  $T=380$  K. All other high symmetry points are shown in Figure S5.

## Discussion

These results imply that the spatial pattern of  $d$ -electron fluctuations is the same as that of the vanadium ion cores, since no enhancement or meaningful differences are observed at resonance. That is,  $d$  electrons and ion cores fluctuate together. Considering Figure 1, the energy landscape that would produce the observed results is the one corresponding to a structural instability [8]. An electronic instability would feature decoupled, independent charge fluctuations coming from preformed electronic dimers. This would manifest as a resonant enhancement, either at the diffuse planes, the critical  $R$  and  $Z$  points -which become reciprocal basis vectors of the M1 and M2 unit cells, respectively- or potentially any of the other high symmetry points.

The incipient lattice instability would not only explain the measurements in Figure 3, but also those in Figure 2. If the lattice is locally fluctuating into the M1/M2 structure, transient dimerization could take place, which would, in turn, localize pairs of carriers, induce antiferromagnetic correlations and favor the formation of singlets. The measured pseudogap [25,26] may arise from the excitation of polarons, formed by the interaction between the deformed lattice and the trapped conduction electron, as is observed in some manganites [49,50].

Interestingly, pre-transitional dynamics are far from being limited to the proximity of the MIT. They set in hundreds of degrees above the transition and show no signs of criticality as the MIT approaches. The magnetic susceptibility varies slowly over a range of almost 700 K, and mid-IR reflectance measurements reveal no significant differences up to 573 K (Figure S6). Similarly, diffuse X-ray scattering patterns remain largely unchanged between 350 K and 500 K (Figure S7) [17]. These observations go in line with our recent report on the anomalous temperature dependence of phonon lifetimes in metallic VO<sub>2</sub> [37], and other studies highlighting the gradual softening of the R-phase lattice [41].

## Conclusions

Using a variety of techniques, we studied the properties of the metallic phase of VO<sub>2</sub>, above the MIT temperature, observing strong electronic and structural pre-transitional fluctuations towards the insulating phase. By measuring diffuse X-ray scattering across the vanadium K-edge, we directly compare the spatial pattern of charge and lattice motion, finding that  $d$ -electrons and ion cores fluctuate jointly. Our results imply that the MIT in VO<sub>2</sub> is triggered by a structural instability and show a new approach to tackle similar open questions in other strongly correlated materials.

## Acknowledgements

We thank Giacomo Mazza, Lucas Korosec, Jean-Marc Triscone and Pablo Alonso González for fruitful discussions. We acknowledge DESY (Hamburg, Germany), a member of the Helmholtz Association HGF, for the provision of experimental facilities. Parts of this research were carried out at beamline P09 at PETRA III. Beamtime was allocated for proposal I-20230723 EC. We also thank the ESRF and ALBA synchrotrons for beamtime allocation and support during the measurements. This work was financed by the Spanish Ministry of Science, Innovation and Universities via the ‘Proyectos de Generación de conocimiento’ grant PID2023-147042NA-I00



and the ‘Ramón y Cajal’ grant RYC-2021-030952-I. Part of the REXS measurements and sample growth were funded by the European Union’s Horizon Europe research and innovation program under grant agreement (ERC, MOTTSWITCH, 101039986). Views and opinions expressed are however those of the authors only and do not necessarily reflect those of the European Union or the European Research Council Executive Agency. Neither the European Union nor the granting authority can be held responsible for them. C.W.R. was supported by the U.S. Office of Naval Research through the NICOP Grant N62909-21-1-2028.

## References

- [1] H. Li *et al.*, Observation of Unconventional Charge Density Wave without Acoustic Phonon Anomaly in Kagome Superconductors  $AV_3Sb_5$  ( $A=Rb, Cs$ ), *Phys. Rev. X* **11**, 031050 (2021).
- [2] E. Dagotto, Open questions in CMR manganites, relevance of clustered states and analogies with other compounds including the cuprates, *New J. Phys.* **7**, 67 (2005).
- [3] J. Diego, A. H. Said, S. K. Mahatha, R. Bianco, L. Monacelli, M. Calandra, F. Mauri, K. Rossnagel, I. Errea, and S. Blanco-Canosa, van der Waals driven anharmonic melting of the 3D charge density wave in  $VSe_2$ , *Nat. Commun.* **12**, 598 (2021).
- [4] X. Zhu, Y. Cao, J. Zhang, E. W. Plummer, and J. Guo, Classification of charge density waves based on their nature, *PNAS* **112**, 2367 (2015).
- [5] M. Imada, A. Fujimori, and Y. Tokura, Metal-insulator transitions, *Rev. Mod. Phys.* **70**, 1039 (1998).
- [6] S. Catalano, M. Gibert, J. Fowlie, J. Iñiguez, J. M. Triscone, and J. Kreisel, Rare-Earth Nickelates  $RNiO_3$ : Thin Films and Heterostructures, *Reports on Progress in Physics* **81** 046501 (2018).
- [7] J. P. Pouget, Basic Aspects of The metal-Insulator Transition in Vanadium Dioxide  $VO_2$ : A Critical Review, *Comptes Rendus Physique* **22**, 37 (2021).
- [8] A. B. Georgescu and A. J. Millis, Quantifying the role of the lattice in metal-insulator phase transitions, *Commun. Phys.* **5**, 135 (2022).
- [9] F. Grandi, A. Amaricci, and M. Fabrizio, Unraveling the Mott-Peierls intrigue in vanadium dioxide, *Phys. Rev. Res.* **2**, 013298 (2020).
- [10] S. Biermann, A. Poteryaev, A. I. Lichtenstein, and A. Georges, Dynamical singlets and correlation-assisted peierls transition in  $VO_2$ , *Phys. Rev. Lett.* **94**, 026404 (2005).
- [11] A. Subedi, O. E. Peil, and A. Georges, Low-energy description of the metal-insulator transition in the rare-earth nickelates, *Phys. Rev. B* **91**, 75128 (2015).
- [12] D. Lee, B. Chung, Y. Shi, G.-Y. Kim, N. Campbell, F. Xue, K. Song, S.-Y. Choi, J. P. Podkaminer, T. H. Kim, P. J. Ryan, J.-W. Kim, T. R. Paudel, J.-H. Kang, J. W. Spinuzzi, D. A. Tenne, E. Y. Tsymbal, M. S. Rzchowski, L. Q. Chen, J. Lee, and C. B. Eom, Isostructural metal-insulator transition in  $VO_2$ , *Science* **362**, 1037 (2018).
- [13] N. F. Mott and Z. Zinamon, The Metal-Nonmetal Transition, *Rep. Prog. Phys.* **33** 881 (1970).
- [14] S. Wall, S. Yang, L. Vidas, M. Chollet, J. M. Glowia, M. Kozina, T. Katayama, T. Henighan, M. Jiang, T. A. Miller, D. A. Reis, L. A. Boatner, O. Delaire, and M. Trigo, Ultrafast disordering of vanadium dimers in photoexcited  $VO_2$ , *Science* **62**, 572 (2018).

- [15] J. H. Park, J. M. Coy, T. Serkan Kasirga, C. Huang, Z. Fei, S. Hunter, and D. H. Cobden, Measurement of a solid-state triple point at the metal-insulator transition in VO<sub>2</sub>, *Nature* **500**, 431 (2013).
- [16] J. B. Goodenough, The two components of the crystallographic transition in VO<sub>2</sub>, *J. Solid State Chem.* **3**, 490 (1971).
- [17] See Supplementary material.
- [18] C. Weber, D. D. O'Regan, N. D. M. Hine, M. C. Payne, G. Kotliar, and P. B. Littlewood, Vanadium dioxide: A peierls-mott insulator stable against disorder, *Phys. Rev. Lett.* **108**, 256402 (2012).
- [19] J. P. Pouget, H. Launois, T. M. Rice, P. Dernier, A. Gossard, G. Villeneuve, and P. Hagenmuller, Dimerization of a linear Heisenberg chain in the insulating phases of V<sub>1-x</sub>Cr<sub>x</sub>O<sub>2</sub>, *Phys. Rev. B* **10**, 1801 (1974).
- [20] W. H. Brito, M. C. O. Aguiar, K. Haule, and G. Kotliar, Metal-Insulator Transition in VO<sub>2</sub>: A DFT/DMFT Perspective, *Phys. Rev. Lett.* **117**, 056402 (2016).
- [21] T. M. Rice, H. Launois, and J. P. Pouget, Comment on "VO<sub>2</sub>: Peierls or Mott-Hubbard? A View from Band Theory", *Phys. Rev. Lett.* **73**, 3042 (1994).
- [22] O. Nájera, M. Civelli, V. Dobrosavljević, and M. J. Rozenberg, Resolving the VO<sub>2</sub> controversy: Mott mechanism dominates the insulator-to-metal transition, *Phys. Rev. B* **95**, 035113 (2017).
- [23] P. B. Allen, R. M. Wentzcovitch, W. W. Schulz, and P. C. Canfield, Resistivity of the high-temperature metallic phase of VO<sub>2</sub>, *Phys. Rev. B* **48**, 4359 (1993).
- [24] M. M. Qazilbash, A. A. Schafgans, K. S. Burch, S. J. Yun, B. G. Chae, B. J. Kim, H. T. Kim, and D. N. Basov, Electrodynamics of the vanadium oxides VO<sub>2</sub> and V<sub>2</sub>O<sub>3</sub>, *Phys. Rev. B* **77**, 115121 (2008).
- [25] M. M. Qazilbash, M. Brehm, B.-G. Chae, P.-C. Ho, G. O. Andreev, B.-J. Kim, S. J. Yun, A. V. Balatsky, M. B. Maple, F. Keilmann, H.-T. Kim, and D. N. Basov, Mott transition in VO<sub>2</sub> revealed by infrared spectroscopy and nano-imaging, *Science* **318**, 1750 (2007).
- [26] T. J. Huffman, P. Xu, M. M. Qazilbash, E. J. Walter, H. Krakauer, J. Wei, D. H. Cobden, H. A. Bechtel, M. C. Martin, G. L. Carr, and D. N. Basov Anisotropic infrared response of vanadium dioxide microcrystals, *Phys. Rev. B* **87**, 115121(2013).
- [27] S. Lee, K. Hippalgaonkar, F. Yang, J. Hong, C. Ko, J. Suh, K. Liu, K. Wang, J. J. Urban, X. Zhang, C. Dames, S. A. Hartnoll, O. Delaire, J. Wu, Anomalously low electronic thermal conductivity in metallic vanadium dioxide, *Science* **355**, 371 (2017).
- [28] A. Sood, X. Shen, Y. Shi, S. Kumar, S. J. Park, M. Zajac, Y. Sun, L.-Q. Chen, S. Ramanathan, X. Wang, W. C. Chueh, and A. M. Lindenberg, Universal phase dynamics in VO<sub>2</sub> switches revealed by ultrafast operando diffraction, *Science* **373**, 352 (2021).
- [29] V. R. Morrison, R. P. Chatelain, K. L. Tiwari, A. Hendaoui, A. Bruhács, M. Chaker, and B. J. Siwick, A photoinduced metal-like phase of monoclinic VO<sub>2</sub> revealed by ultrafast electron diffraction, *Science* **346**, 445 (2014).
- [30] A. S. McLeod, E. van Heumen, J. G. Ramirez, S. Wang, T. Saerbeck, S. Guenon, M. Goldflam, L. Andereg, P. Kelly, A. Mueller, M. K. Liu, Ivan K. Schuller, and D. N. Basov, Nanotextured phase coexistence in the correlated insulator V<sub>2</sub>O<sub>3</sub>, *Nat. Phys.* **13**, 80 (2017).

- [31] D. J. Lahneman, T. Slusar, D. B. Beringer, H. Jiang, C. Y. Kim, H. T. Kim, and M. M. Qazilbash, Insulator-to-metal transition in ultrathin rutile VO<sub>2</sub>/TiO<sub>2</sub>(001), *NPJ Quantum Mater.* **7**, 72 (2022).
- [32] C. W. Rischau, X. He, G. Mazza, S. Gariglio, J. M. Triscone, P. Ghosez, and J. del Valle, Oxygen isotope effect in VO<sub>2</sub>, *Phys. Rev. B* **107**, 115139 (2023).
- [33] Y. Kalcheim, N. Butakov, N. M. Vargas, M. H. Lee, J. Del Valle, J. Trastoy, P. Salev, J. Schuller, and I. K. Schuller, Robust Coupling between Structural and Electronic Transitions in a Mott Material, *Phys. Rev. Lett.* **122**, 057601 (2019).
- [34] G. J. Paez, C. N. Singh, M. J. Wahila, K. E. Tirpak, N. F. Quackenbush, S. Sallis, H. Paik, Y. Liang, D. G. Schlom, T.-L. Lee, C. Schlueter, W.-C. Lee, and L. F. J. Piper, Simultaneous Structural and Electronic Transitions in Epitaxial VO<sub>2</sub>/Ti O<sub>2</sub> (001), *Phys. Rev. Lett.* **124**, 196402 (2020).
- [35] L. Vidas, D. Schick, E. Martínez, D. Perez-Salinas, A. Ramos-Álvarez, S. Cichy, S. Batlle-Porro, A. S. Johnson, K. Hallman, R. F. Haglund Jr., and S. Wall, Does VO<sub>2</sub> Host a Transient Monoclinic Metallic Phase? *Phys. Rev. X* **10**, 031047 (2020).
- [36] M. O. Krause and J. H. Oliver, Natural widths of atomic K and L levels, K $\alpha$  X-ray lines and several KLL Auger lines, *J. Phys. Chem. Ref. Data* **8**, 329 (1979).
- [37] C. W. Rischau, A. Korshunov, V. Multian, S. A. Lopez-Paz, C. Huang, L. Varbaro, J. Teyssier, Y. Kalcheim, S. Gariglio, A. Bossak, J.-M. Triscone, J. del Valle, Anomalous temperature dependence of phonon lifetimes in metallic VO<sub>2</sub>, *Phys. Rev. B* **109**, 094122 (2024).
- [38] L. Baldassarre, A. Perucchi, D. Nicoletti, A. Toschi, G. Sangiovanni, K. Held, M. Capone, M. Ortolani, L. Malavasi, M. Marsi, P. Metcalf, P. Postorino, and S. Lupi, Quasiparticle evolution and pseudogap formation in V<sub>2</sub>O<sub>3</sub>: An infrared spectroscopy study, *Phys. Rev. B* **77**, 113107 (2008).
- [39] S. Mugiraneza and A. M. Hallas, Tutorial: A Beginner's Guide to Interpreting Magnetic Susceptibility Data with the Curie-Weiss Law, *Comm. Phys.* **5**, 95 (2022).
- [40] M. A. Davenport, M. J. Krogstad, L. M. Whitt, C. Hu, T. C. Douglas, N. Ni, S. Rosenkranz, R. Osborn, and J. M. Allred, Fragile 3D Order in V<sub>1-x</sub>Mo<sub>x</sub>O<sub>2</sub>, *Phys. Rev. Lett.* **127**, 125501 (2021).
- [41] J. D. Budai, J. Hong, M. E. Manley, E. D. Specht, C. W. Li, J. Z. Tischler, D. L. Abernathy, A. H. Said, B. M. Leu, L. A. Boatner, R. J. McQueeney, and O. Delaire, Metallization of vanadium dioxide driven by large phonon entropy, *Nature* **515**, 535 (2014).
- [42] A. Carpi, Lattice dynamics of VO<sub>2</sub> above the metal insulator transition, Thesis, Politecnico Di Milano (2015).
- [43] G. Ghiringhelli, M. Le Tacon, M. Minola, S. Blanco-Canosa, C. Mazzoli, N.B. Brookes, G.M. De Luca, A. Frano, D. G. Hawthorn, F. He, T. Loew, M. Moretti Sala, D.C. Peets, M. Salluzzo, E. Schierle, R. Sutarto, G. A. Sawatzky, E. Weschke, B. Keimer, and L. Braicovich, Long-range incommensurate charge fluctuations in (Y,Nd)Ba<sub>2</sub>Cu<sub>3</sub>O<sub>6+x</sub>, *Science* **337**, (2012).
- [44] L. Paolasini, C. Vettier, F. de Bergevin, F. Yakhou, D. Mannix, A. Stunault, W. Neubeck, M. Altarelli, M. Fabrizio, P. A. Metcalf, and J. M. Honig, Orbital occupancy order in V<sub>2</sub>O<sub>3</sub>: Resonant X-Ray Scattering results, *Phys. Rev. Lett.* **82**, 4719 (1999).

- [45] R. Comin and A. Damascelli, Resonant X-Ray Scattering Studies of Charge Order in Cuprates, *Ann. Rev. Cond. Matt. Phys.* **7**, 369 (2016).
- [46] J. R. Soh, E. Schierle, D. Y. Yan, H. Su, D. Prabhakaran, E. Weschke, Y. F. Guo, Y. G. Shi, and A. T. Boothroyd, Resonant x-ray scattering study of diffuse magnetic scattering from the topological semimetals  $\text{EuCd}_2\text{As}_2$  and  $\text{EuCd}_2\text{Sb}_2$ , *Phys. Rev. B* **102**, 014408 (2020).
- [47] I. H. Hwang, Z. Jin, C. I. Park, and S. W. Han, The influence of structural disorder and phonon on metal-to-insulator transition of  $\text{VO}_2$ , *Sci. Rep.* **7**, 14802 (2017).
- [48] N. B. Aetukuri, A. X. Gray, M. Drouard, M. Cossale, L. Gao, A. H. Reid, R. Kukreja, H. Ohldag, C. A. Jenkins, E. Arenholz, K. P. Roche, H. A. Dürr, M. G. Samant, and S. S. P. Parkin, Control of the metal–insulator transition in vanadium dioxide by modifying orbital occupancy, *Nat. Phys.* **9**, 661 (2013).
- [49] C. Franchini, M. Reticcioli, M. Setvin, and U. Diebold, Polarons in Materials, *Nature Rev. Mater.* **6**, 560 (2021).
- [50] M. Quijada, J. Černe, J. Simpson, and H. Drew, Optical conductivity of manganites: Crossover from Jahn-Teller small polaron to coherent transport in the ferromagnetic state, *Phys. Rev. B* **58**, 16093 (1998).

# Supplementary information

## 1. Experimental methods

### Crystal growth, transport, and susceptibility measurements.

VO<sub>2</sub> single crystals were fabricated using the self-flux method, annealing V<sub>2</sub>O<sub>5</sub> powder (99.95 %, Aldrich) for 24 hours at 1000° C in a horizontal tube furnace under an Argon gas flow. High-quality single crystals with lengths up to several mm can be obtained this way. Typically, 5 grams of V<sub>2</sub>O<sub>5</sub> powder yield around 10 mg of hundreds of VO<sub>2</sub> crystals. Most of them are smaller than 100 μm, but many of them have lengths up to 1-2 mm and are large enough to be easily manipulated with tweezers. The crystals are needle-shaped, with the long axis oriented along (001)<sub>R</sub>, and their side faces perpendicular to the (110)<sub>R</sub> direction

Transport measurements were done using a four-probe geometry in a Lakeshore TTPX probe station. Silver paste was used to contact the crystals. Magnetic susceptibility was measured using vibrating sample magnetometry in a EV9 magnetometer. 10.8 mg of VO<sub>2</sub> crystals were used. For susceptibility measurements, the crystals were partially crushed into smaller pieces to avoid alignment into a preferential direction, and they were kept under an N<sub>2</sub> atmosphere during the measurement to avoid oxidation at high temperatures.

### Fourier-transform Infrared reflectivity (FTIR) measurements.

FTIR measurements were done at the BL01-MIRAS beamline at the ALBA Synchrotron. We used a reflection geometry with a Hyperion 3000 microscope coupled to a Vertex 70 spectrometer. A Linkam stage was used to warm the samples above room temperature. A gold reference was used to normalize the sample spectra.

### Hard X-ray total scattering measurements.

The total X-ray scattering measurements shown in Figure 3 and S7 were collected on the ID28 beamline at the European Synchrotron Radiation Facility (ESRF).

A VO<sub>2</sub> crystal, glued with epoxy to the sample holder was measured in transmission geometry. A photon energy of 15.8 keV was used, and scattered radiation was collected with a Pilatus 2D detector. A N<sub>2</sub> heat blower was used to warm up the sample while preventing its oxidation.

### Resonant Elastic X-ray scattering (REXS).

X-ray diffraction across the vanadium K-edge, shown in Figures 4, S4 and S5, was performed at the P09 beamline at PETRA III at DESY.

A VO<sub>2</sub> single crystal was glued onto the sample holder using silver paste. The sample holder was screwed into the cold finger of an ARS cryostat, isolated from the outside using a Beryllium dome and steel shroud, and then pumped down to 10<sup>-6</sup> mbar for cryogenic operations. A Lakeshore 340 temperature controller was used to control the sample temperature.

Because of the low penetration depth at 5 keV and given the relatively large size of our crystals, a reflection Bragg geometry was used to measure the scattered intensity. Given the low momentum of photons at 5.48 keV and the reflection geometry, high  $2\theta$  angles ( $>100^\circ$ ) were needed to reach the few available high symmetry points. Measurements were performed using an avalanche photodiode point detector to detect the weak features of diffuse scattering, and a PG001 analyzer for suppressing the fluorescence background and for polarization analysis. The analyzer was used for all measurements except the fluorescence curve of Figure 4b. Measurements consisted on: i) fixed energy hkl line scans through reciprocal space (Figure 4a) or ii) fixed  $k$  energy scans at several reciprocal space points (Figures 4b, S4 and S5). Energy resolution was around 0.7 eV.

## 2. Further REXS measurements

Data shown in Figures 4 and S5 were collected with the incident beam electric field pointing parallel or almost parallel to the rutile  $c$  axis (with a  $0^\circ$ - $12^\circ$  offset, depending on the specific point in reciprocal space), as shown in the inset of Figure S4a. A  $\sigma$ - $\sigma'$  configuration was used, that is, the incoming beam was polarized perpendicular to the scattering plane, and the same polarization component of the scattered light was measured. However, other azimuths and polarizations were also measured, and are shown in Figure S4.

Figure S4a and S4b show the  $\sigma$ - $\sigma'$  and  $\sigma$ - $\pi'$  signals measured at the  $M$  point for two different azimuths: with the electric field parallel and perpendicular to rutile  $c$ -axis, respectively. The measurement geometries are schematically represented in the insets. The results are similar in both cases: the  $\sigma$ - $\sigma'$  channel signal drops across the K-edge, following an absorption-dominated behavior, without any resonant enhancements. A similar behavior is observed at the  $R$  point for the two azimuths.

We see a small  $\sigma$ - $\pi'$  step starting at the K pre-edge, indicating a slight rotation of the scattered light. The signal is much weaker than that of the  $\sigma$ - $\sigma'$  channel. We see this feature in every reciprocal space point that we measured, including all high symmetry points and a random background point (Figure S4d). We also see it for the two sample azimuths that we measured at the  $M$  and  $R$  points. The signal increment across the step is always around 150-200 cps, independent of the measurement geometry. This lack of orientation and momentum dependence rules out that any electronic ordering is contributing to this signal, and points to an intrinsic background effect or an artifact.

### 3. Supplementary figures

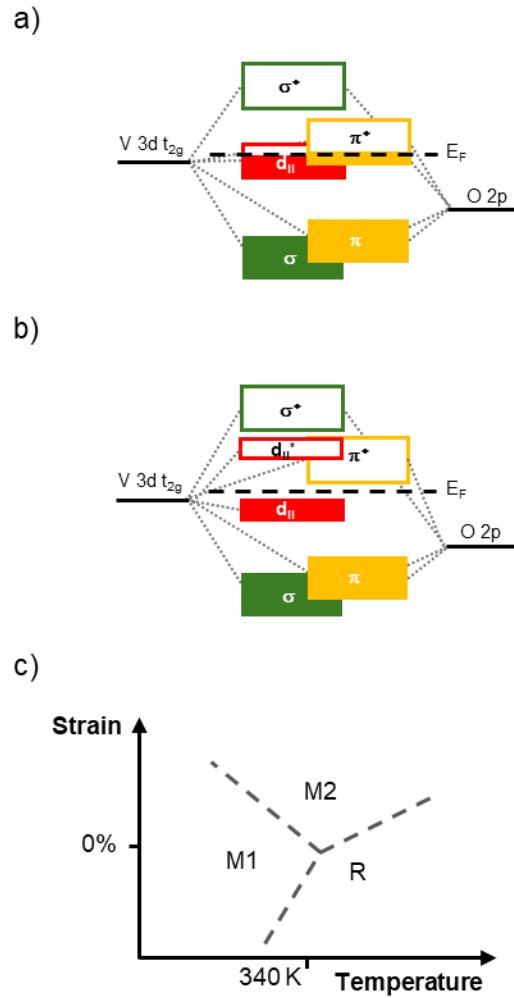


Figure S1. Schematic representation of the  $\text{VO}_2$  band structure proposed by Goodenough [16] for the a) rutile and b) monoclinic phases. There are three vanadium  $t_{2g}$  orbitals. One of them ( $d_{||}$ ) is oriented along the  $c$ -rutile axis, pointing towards the nearest vanadium atom (See lattice structure in Figure S2). The other two hybridize with the O 2p orbitals, forming a pair of bonding and antibonding  $\sigma$  and  $\pi$  orbitals. In the metallic rutile phase, both the  $d_{||}$  and  $\pi^*$  orbitals are crossed by the Fermi surface. There is a slight orbital polarization, with the  $d_{||}$  orbital laying lower and having higher occupancy. The structural transition into the monoclinic phase lifts the  $\pi^*$  orbital, leaving the  $d_{||}$  half-filled. Dimerization splits  $d_{||}$  into a bonding-antibonding pair, yielding an insulating phase. Unfortunately, the  $\sigma$  and  $\pi$  notation commonly adopted to designate the  $\text{VO}_2$  valence orbitals is the same as the one used to distinguish the light polarization in REXS experiments, so we caution the reader to distinguish between both. c) Schematic representation of the  $\text{VO}_2$  phase diagram as a function of strain and temperature [15].

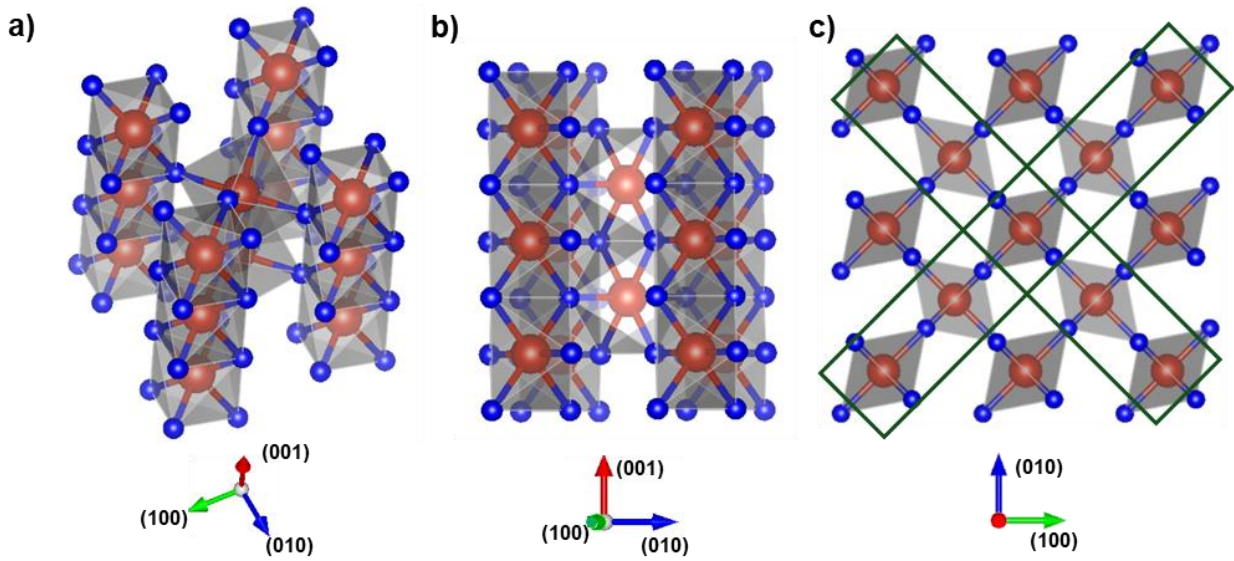


Figure S2. Structure of  $RVO_2$ , visualized along different directions as indicated by the red/blue/green arrows. Red balls represent vanadium atoms, and blue balls are oxygens.  $VO_6$  octahedra are outlined by transparent grey surfaces. The dark green rectangles in c) outline the  $(\pm 1 \pm 1 0)_R$  planes where structural correlations are strongest [40].



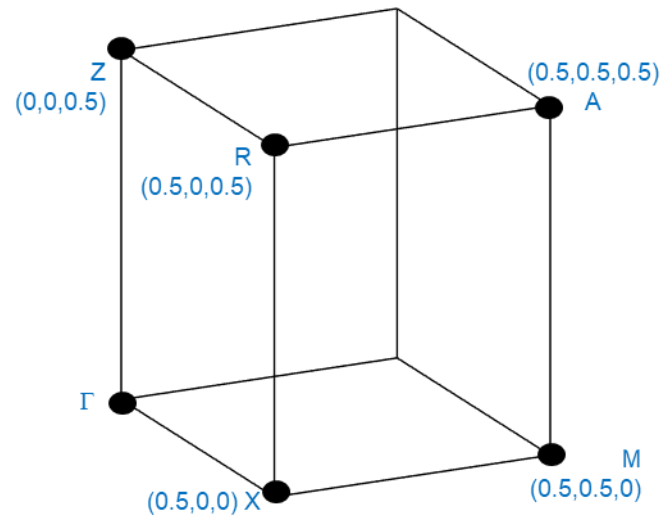


Figure S3. Brillouin zone of the tetragonal rutile structure of the R phase. Black dots show the high symmetry points.

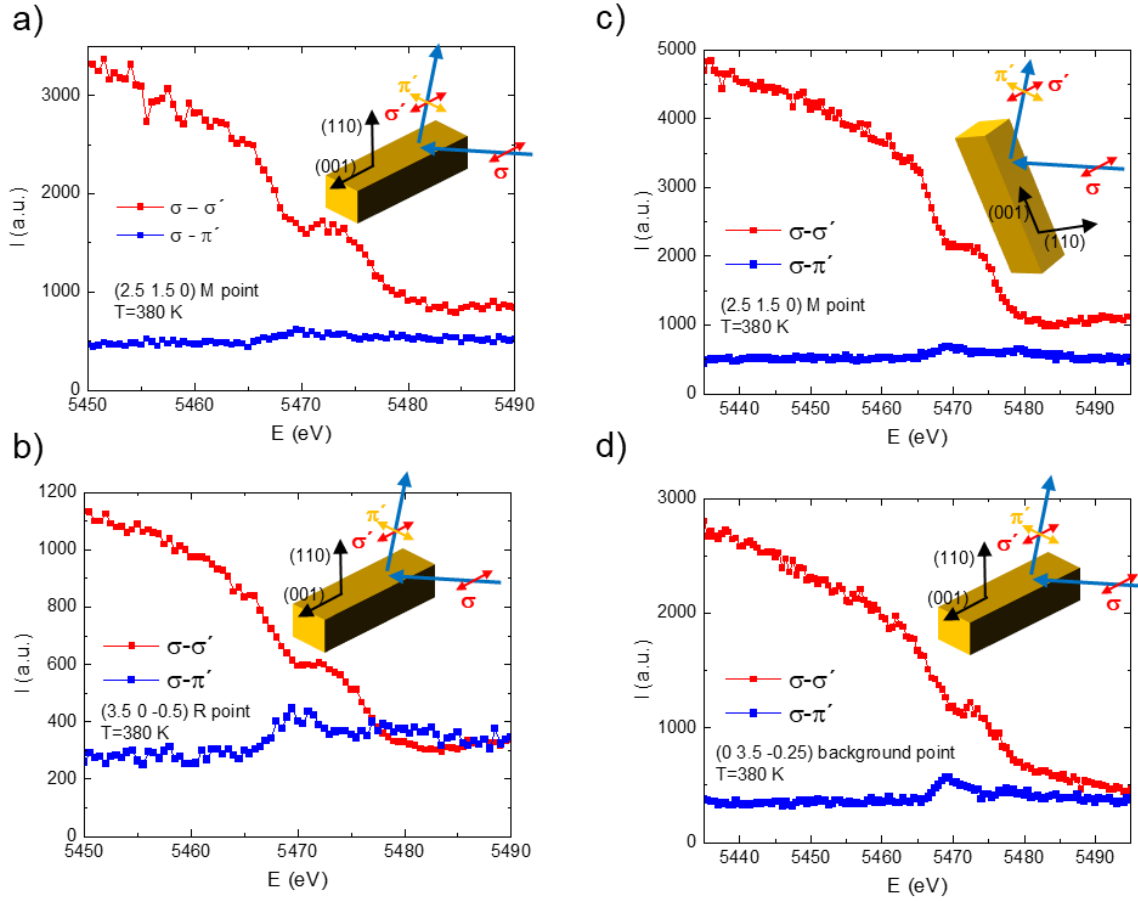


Figure S4. X-ray intensity vs energy across the vanadium K-edge measured at 380 K in different geometries and at different reciprocal space points. a) and b) are measured at the  $M$  point with the incoming beam polarized parallel (a) and perpendicular (b) to the rutile  $c$ -axis. c) and d) are measured with the light polarized almost parallel to the rutile  $c$ -axis, at the R point (c) and at a background point (d). In all cases, both the unrotated  $\sigma$ - $\sigma'$  and the  $90^\circ$  rotated  $\sigma$ - $\pi'$  channels are shown, in red and blue, respectively. The schematic inset figures show the measurement geometry. The brown block represents the  $\text{VO}_2$  needles, the red double arrows represent light that is polarized perpendicular to the scattering plane ( $\sigma$  or  $\sigma'$ ), and the orange double arrow represent scattered light that is polarized parallel to the scattering plane ( $\pi'$ ).

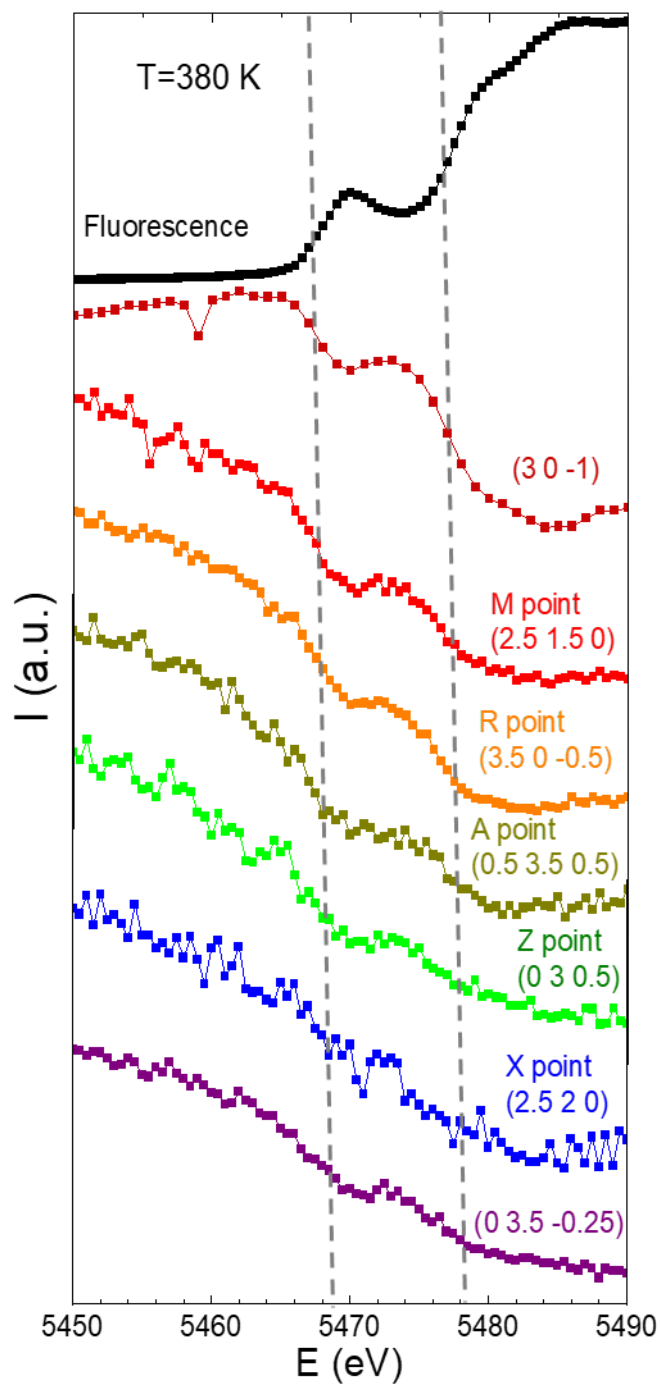


Figure S5. X-ray intensity vs photon energy across the K-edge for several points in reciprocal space: the Bragg (3 0 -1) reflection, all high symmetry points of the R structure and the background point (0 3.5 - 0.25). T=380 K. A  $\sigma$ - $\sigma'$  measurement geometry was used, with the incoming light polarized parallel or almost parallel to the rutile  $c$ -axis.

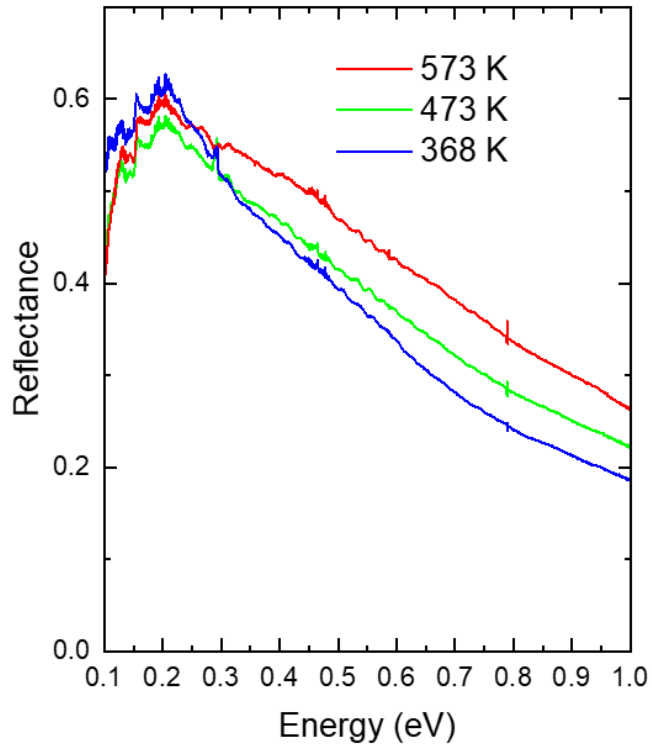


Figure S6. Infrared reflectance vs photon energy, with light polarized along the c axis. Three temperatures above the MIT are shown.

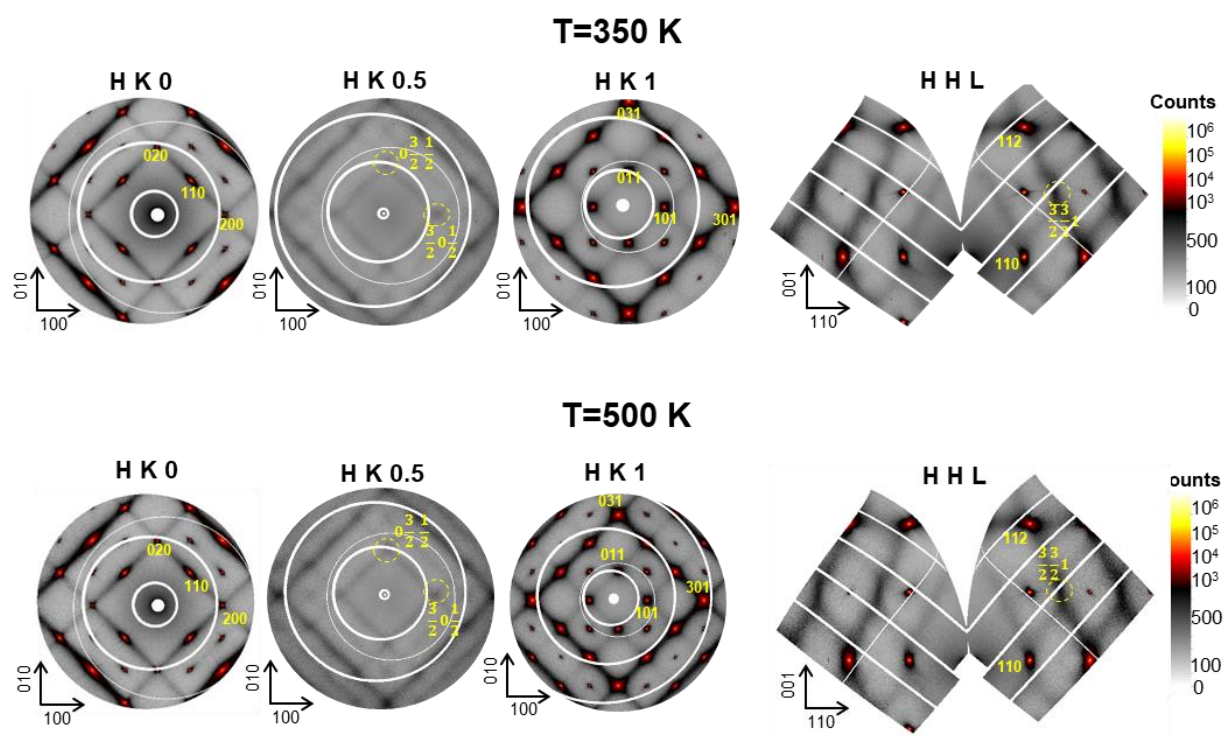


Figure S7. X-ray total scattering in different slices of the reciprocal space: HK0, HK0.5, HK1 and HHL. Two temperatures are shown: 350 K in the upper panels and 500 K in the bottom panels.